ResearchGate

See discussions, stats, and author profiles for this publication at: https://www.researchgate.net/publication/223482711

Recrystallization and diffusion in sodium-implanted silicon

ARTICLE *in* THIN SOLID FILMS · FEBRUARY 1997

Impact Factor: 1.76 · DOI: 10.1016/S0040-6090(96)09287-5

CITATIONS
6

READS
13

6 AUTHORS, INCLUDING:

Wei-Hua Wang
Chinese Academy of Sciences
434 PUBLICATIONS **12,358** CITATIONS
SEE PROFILE

Wolfgang Bolse
Universität Stuttgart
129 PUBLICATIONS **1,994** CITATIONS
SEE PROFILE

J. Keinonen
University of Helsinki
371 PUBLICATIONS **7,327** CITATIONS
SEE PROFILE

Available from: Wei-Hua Wang
Retrieved on: 27 January 2016

ELSEVIER

Thin Solid Films 295 (1997) 169–177

thin solid films

Recrystallization and diffusion in sodium-implanted silicon

W.H. Wang [a], W. Bolse [a,*], C. Illgner [a], K.P. Lieb [a], J. Keinonen [b], J.C. Ewert [c]

[a] *II Physikalisches Institut and Sonderforschungsbereich 345, University of Gottingen, D-37073 Göttingen, Germany*

[b] *Accelerator Laboratory, P.O. Box 43, FIN-00014 University of Helsinki, Helsinki, Finland*

[c] *Institut für Metallphysik and Sonderforschungsbereich 345, University of Gottingen, D-37073 Gottingen, Germany*

Received 26 March 1996; accepted 22 August 1996

Abstract

We have investigated the thermally induced recrystallization of silicon amorphized by sodium-ion irradiation and the diffusion of the implanted Na atoms. Si(100) wafers were irradiated at 77 and 300 K with 50–200 keV Na^+ ions to fluences of 10^{15}–10^{17} cm^{-2} and then furnace annealed in the temperature range of 473–943 K. The recrystallization of the amorphous Si and the migration of Na were investigated by Rutherford backscattering spectrometry combined with channeling and by resonant nuclear reaction analysis. At a Na fluence of 1×10^{15} cm^{-2} annealing results in fast and almost complete solid-phase epitaxial regrowth (SPEG) whereas a competition between epitaxial and polycrystalline recrystallization was observed for fluences at or above 10^{16} cm^{-2}. The transition from epitaxial to polycrystalline regrowth, observed when the recrystallization front has reached a depth of high Na concentration, was attributed to the retardation of the SPEG due to pronounced Na segregates located near the amorphous/crystalline interface. During further annealing these segregates then dissolve by grain boundary diffusion of Na towards the surface through the polycrystalline layer. At the critical temperature $T_c = 885(30)$ K, half of the implanted Na content has diffused out of the sample. Hydrogen was observed to be trapped in the amorphized region during annealings at temperatures of 673–723 K, while above it is again released. © 1997 Elsevier Science S.A.

Keywords: Crystallization; Ion implantation; Silicon; Sodium

1. Introduction

Ion beams of several keV to several MeV energy can be used to deposit foreign atoms into a host material at almost any concentration and a wide range of controllable depth distributions. The electronic industry has taken advantage of this fact already for more than two decades to introduce very small amounts of electrically active dopants into semiconducting materials, but also buried compound layers with properties different from those of the host matrix can be produced. Yet, ion implantation is always accompanied by the generation of point defects, defect agglomerates or even amorphous volumes. In many cases this is an unwanted side effect and may significantly disturb the property alterations wanted to be achieved by the implantation process. An easy approach to get rid of the radiation damage is to anneal the sample at sufficiently high temperatures after ion implantation has taken place. However, in order to optimize the annealing conditions and to finally approach the desired microstructure and related properties, detailed studies of the thermally induced recrystallisation and migration processes are required.

Amorphous layers, produced by ion bombardment in the near-surface region of silicon single crystals, recrystallize by solid-phase epitaxial growth (SPEG) when the sample is heated in a furnace to temperatures above about 773 K [1,2]. SPEG can be easily examined by Rutherford backscattering spectrometry in channeling geometry (RBS-C). The recrystallization kinetics has been investigated in considerable detail after low-dose heavy-ion irradiation [3]. It has been demonstrated that the recrystallization rates dramatically depend on the sample orientation [4] and on the nature and amount of the implanted impurities [5–7]. In particular, regrowth of Si(111) is slow whereas regrowth of Si(100) proceeds more rapidly and leads to an almost perfect epitaxial layer. Certain implanted impurities, such as As or In, were found to speed up the SPEG process as long as their concentration at the recrystallization front does not exceed some 0.1 at.% [8–10]. Beyond this limit, the regrowth rate was found to drop below the one observed in self-ion irradiated impurity-free Si. More reactive ions, like O, N and C, retard the recrystallization already at low concentrations [7]. The amount of impurities incorporated into the epitaxial layer (the

* Corresponding author.

0040-6090/97/$17.00 © 1997 Elsevier Science S A All rights reserved
PII S0040-6090(96)09287-5

metastable solid solubility limit) was found to strongly decrease with increasing covalent radius of the impurity atom. Lattice location measurements by means of RBS-C proved that the impurities were located on substitutional sites [3,11].

Phenomenological models of SPEG have been proposed and observed to be successful in providing an explanation for the regrowth kinetics [12–17]. However, many details of the SPEG mechanism are not yet well understood, especially the dependence on the concentration and diffusion constants of dopants. In particular, the regrowth and annealing behavior of silicon in the presence of high impurity concentrations of some atomic percent appears to be of a complex nature.

In the present work, we report on a combined study of RBS-C and resonant nuclear reaction analysis (RNRA) for Si(100) implanted with Na ions. The use of ^{23}Na atoms as implants results from various reasons. The depth profile of this light mono-isotopic element can be easily measured with the resonant nuclear reaction ^{23}Na(p,γ)^{24}Mg. If we make use of the 308.75 keV resonance [18], the concentration distribution of Na atoms can be measured with a depth resolution of typically 10 nm down to a minimum concentration of about 0.1 at.% and no disturbing γ-ray signals arise from nuclear reactions between the probing proton beam and the Si nuclei of the sample. RNRA thus provides a non-destructive and very sensitive method to measure depth profiles of Na atoms over quite a large dose range of the implanted Na ions which by no means would be accessible to RBS, used in previous studies on the amorphization and recrystallization of ion-irradiated Si.

Furthermore, Na is essentially insoluble in Si, the equilibrium solubility being 1.2×10^{18} Na cm^{-3} at 840 K, that is 2.4×10^{-3} at.% [19,20]. Its covalent radius is about 1.3 times larger than that of Si and thus, according to Ref. [11], its metastable solubility during epitaxial recrystallization of Si should be about 0.04 at.% at 773 K. Compound formation of the implanted Na and Si during subsequent annealing is not expected. Thus, diffusion, segregation and release of Na into the vacuum during or after recrystallization should become easily observable.

Previous studies on Na diffusion after implantation into polycrystalline metals have given evidence of a multi-stage process in which Na first segregates into the available open volume [21]. This can be either due to vacancy-type defects created in the collision cascades of the Na ions during implantation (correlated radiation damage) or to the damage produced by post-implanted ions (non-correlated damage). It can be further due to the lattice mismatch at the interfaces in layered structures. In this context, recent work by Haussalo et al. [22] on Na implantation and migration in Ni/Si and Ni/SiO_2 bilayer couples should be mentioned. It was found that migrating Na might be trapped at the Ni/SiO_2 interface. In Ni/Si the situation was more complicated because the interface was dissolved due to Ni-silicide formation.

In the previous studies on the recrystallization of ion-implanted Si, hydrogen trapping at open volume defects and a possible role of H atoms on the observed phenomena, have to our knowledge not yet been investigated. In our studies on the polycrystalline metals [21] and Ni/Si and Ni/SiO_2 bilayer couples [22], hydrogen trapping was observed to give additional information on the annealing processes.

It was, therefore, tempting to search for correlations between the recrystallization of silicon and the amount and transport properties of the implanted Na atoms, as well as the behavior of hydrogen during the recovery of the Si crystal.

2. Experimental procedure

Si(100) wafers of 0.5 mm thickness were irradiated at room temperature (RT) with 50 keV Na^+ ions to fluences of 1×10^{15}, 1×10^{16}, and 1×10^{17} cm^{-2}. The implantations were carried out at the Göttingen 500 kV implanter IONAS [18]. In all cases the beam current was kept below 2 μA cm^{-2} in order to avoid beam heating. Homogeneous irradiation over an area of 10×10 mm^2 was achieved by an electrostatic x–y beam sweeping system. After irradiation the samples were heated in a furnace in flowing argon at temperatures between 753 and 853 K. The temperature was controlled by a thermocouple, which was attached to the sample surface, and could be fixed within about 2 K. The annealings were carried out for 0.5, 1, 2 and 4 h.

RBS-C was used to monitor both the amorphization due to the ion irradiation and the recrystallization due to thermal annealing. The RBS-C measurements were carried out at RT using the 900 keV α-particle beam of the Göttingen IONAS implanter. The backscattering spectra were taken with a Si surface barrier detector positioned in the plane formed by the beam and the tilt axis of the goniometer at an angle of 165° with respect to the beam direction. The energy resolution of the detector was typically 12 keV at full width at half-maximum (FWHM). A detailed description of the set-up [23] and the techniques [24] are given elsewhere. RNRA was performed utilizing the nuclear reaction ^{23}Na(p,γ)^{24}Mg at the very narrow 308.75 keV resonance, whose width is less than 20 eV [18]. Because of this narrow resonance width and the small energy spread of the proton beam, about 50 eV at the resonance energy, the depth resolution of the probing proton beam was mainly due to the proton energy straggling in the sample. It is approximately 20 nm at the depth of 100 nm which corresponds to the center of the as-implanted Na profile. A typically 2 μA proton beam having a diameter of 3 mm was focused on the Na implanted area of the sample. The target was cooled to 77 K (LNT). Each Na profile, extending over 200 nm in depth, was measured with about 20 different energy values of the proton beam. For each proton energy the accumulated charge was 0.5 mC. The γ-radiation emitted after the capture process was measured in a 15 cm (dia.) $\times$ 12 cm NaI(Tl) detector shielded against background radiation with a 5 cm thick lead shielding. A detailed description of this technique can be found in Refs. [21,25,26].

A second series of measurements was devoted to study the outdiffusion of Na as a function of the annealing temperature. Fluences of 1×10^{16} Na^+ ions cm^{-2} were implanted at RT at an energy of 60 keV by means of the 60 kV mass separator at the University of Helsinki and, at LNT, fluences of 1×10^{17} cm^{-2} with an energy of 200 keV by means of the IONAS implanter in Göttingen. The samples were annealed in vacuum (4×10^{-7} mbar) at temperatures between 473 and 943 K for 1 h each and the Na profiles were measured utilizing RNRA as described above.

Concentration distributions of hydrogen atoms in these samples were measured by means of RNRA along with the 6.48 MeV resonance in the reaction $^1H(^{15}N,\alpha\gamma)^{12}C$. For further details see Ref. [27]. The 150 particle nA beam of $^{15}N^{++}$ ions was supplied by the 5 MV tandem accelerator EGP-10-II at the Accelerator laboratory of the Helsinki University.

In Fig. 1 the Na profiles taken after 60 keV (RT) and after 200 keV (LNT) implantation and after annealings up to 943 K are shown. The depth ($x(E_p)$) and concentration ($c(x)$) scales were evaluated by using the proton stopping power function (dE/dx) for Si given by Ziegler [28]. For approximately constant (dE/dx), as is the case in the energy intervals used in the present study, one obtains:

$$x(E_p) = (E_p - E_r)/(dE/dx)$$

$$c(x) = KN_\gamma(dE/dx)$$

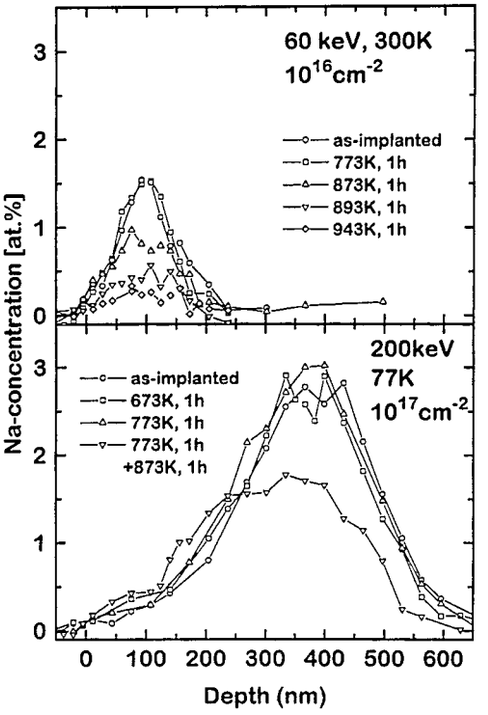

Fig. 1. Na profiles in Si, taken after implantation and subsequent 1 h vacuum annealings for samples implanted with: (a) 1×10^{16} Na^+ cm^{-2} at 60 keV and 300 K, (b) 1×10^{17} Na^+ cm^{-2} at 200 keV and 77 K.

E_p denotes the proton-beam energy, E_r the resonance energy and N_γ the gamma ray yield per incident proton. The normalization constant K depends on the resonance strength and the detection efficiency and was determined with a standard sample of known Na content. The alterations of (dE/dx) due to the small Na content (<3 at.%) was neglected in this calculation since it was not noticed to have any significant effect on the deduced depth and concentration values. The measured Na profiles after implantation have a mean range of $R=110$ nm and a width of $\Delta R=105$ nm (FWHM) for the 60 keV implantation and $R=380$ nm, $\Delta R=280$ nm for 200 keV implantation energy. The corresponding numbers of the profiles calculated with the program TRIM95 [29] are $R=120$ nm, $\Delta R=110$ nm, $R=400$ nm and $\Delta R=260$ nm, respectively, in good agreement with the experiment.

3. Results and discussion

3.1. Amorphization of silicon

Silicon can be easily amorphized by Na-ion bombardment, as was recently shown by Bolse et al. [30] who found a critical fluence of 1.5×10^{14} cm^{-2} for the onset of amorphization during 50 keV Na bombardment of Si(100) at LNT. After bombardment with about twice this critical fluence a coherent amorphous layer was found, which extended to the surface and had a thickness of about 150 nm, and after 1×10^{16} Na cm^{-2} the amorphous layer had grown to about 200 nm thickness. In case of RT irradiation, the critical fluence might be slightly shifted to higher values due to dynamic annealing effects. However, the Na fluences used in the present study still result in complete amorphization of the Si surface, as is illustrated in Figs. 2 and 3. Fig. 2 shows RBS-C spectra measured in a random direction and with the beam aligned along the (100) crystallographic axis for a non-irra-

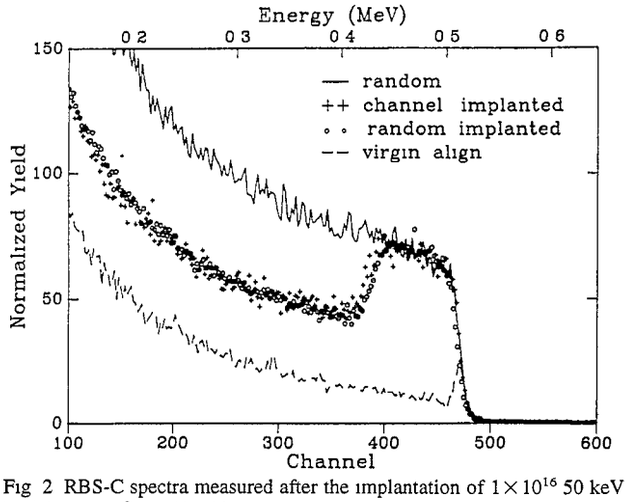

Fig 2 RBS-C spectra measured after the implantation of 1×10^{16} 50 keV Na^+ ions cm^{-2} into Si(100) under random and (001) channeling injection. For comparison a random and an aligned spectrum of a virgin sample are also shown

diated sample (virgin aligned) in comparison with the aligned spectra taken after the implantation of a 10^{16} cm^{-2} 50 keV Na ion beam either aligned or misaligned by 5° with respect to the (100) channel. These latter two spectra overlap fairly well with a slightly larger amorphized layer produced after the channeling implantation. The latter is due to the somewhat larger ion range because of the reduced stopping power in the channel direction at the beginning of the implantation.

Fig. 3 illustrates the amorphization induced by different Na-ion fluences. The relative RBS-C yields, normalized to the "random" value, of a non-irradiated sample in the (100)-aligned and the random orientation are compared with those obtained from samples irradiated to fluences of 1×10^{15}, 1×10^{16}, and 1×10^{17} 50 keV Na^+ ions cm^{-2}, measured in the aligned direction. In all cases an amorphous layer has formed, which extends to the surface and which has a thickness of 145 nm in the case of an implanted fluence of 1×10^{15} Na^+ ions cm^{-2}, 175 nm for 1×10^{16} Na^+ ions cm^{-2}, and about 200 nm for 1×10^{17} Na^+ ions cm^{-2}. Note the rather sharp amorphous/crystalline (a/c) interfaces. At the fluence of 1×10^{17} cm^{-2} the peak to be observed in the spectrum around 180 nm is due to the overlap of the Si signal with the backscattering yield from the implanted Na atoms. Note that the backscattering yields of Si and Na at a given backscattering energy correspond to different depths because of the higher kinematic energy loss of the analysing α-particles when colliding with Na atoms as compared to collisions with Si atoms. Therefore, the rear edge of the composed RBS spectrum does not correspond to the a/c interface in Si but reflects the sum of the step-like Si signal from the interfacial region and the Na signal from the Gaussian-like implantation profile in front of the interface, with the maximum of the latter and the step being located at almost the same energy. The backscattering yields from the crystalline regions behind the amorphous layers are subject to dechanneling of the probing beam in the amorphized front layer.

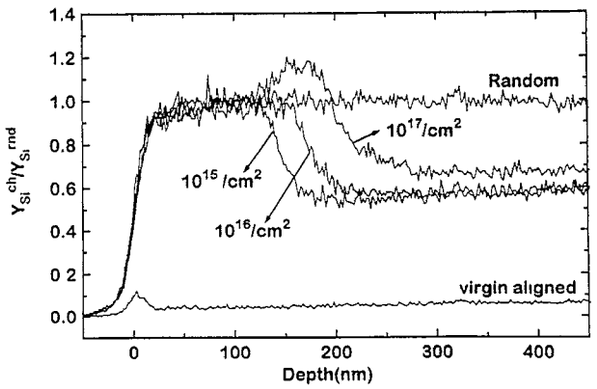

Fig 3. RBS-C spectra, normalized to the "random" yield, measured after the implantation of 1×10^{15}, 1×10^{16}, and 1×10^{17} 50 keV Na^+ ions cm^{-2} into c-Si. The given depth scale refers to α-particles scattered at Si atoms.

3.2. Recrystallization of silicon

3.2.1. Low-fluence implantation

RBS-C spectra measured after implantation of 1×10^{15} Na^+ ions cm^{-2} into Si(100) and annealing the samples for 1 and 2 h at 773 K in an argon atmosphere are shown in Fig. 4(a). After 1 h annealing the amorphous layer has disappeared indicating complete epitaxial regrowth. However, these spectra still differ from that taken before irradiation ("virgin aligned"), i.e. exhibit a slightly higher backscattering yield. This difference has become smaller but has not fully disappeared after 2 h annealing. We attribute this remaining disorder to extended defects such as dislocations and dislocation loops, which do not significantly act as direct backscattering centers but cause dechanneling of the probing beam [31]. The epitaxial recrystallization also coincides with a change in the surface color from gray–white, indicating the amorphous structure, to a shiny gray crystalline appearance.

For the same sample, Fig. 4(b) illustrates the Na concentration profiles as measured with RNRA after implantation and after 1 h annealing. After annealing Na has partly migrated out of the implanted zone and is found at the surface. As can be seen in the RBS-C spectra, a small amount of oxygen is present at the samples surface. Since Na is known to strongly react with oxygen [32] we conclude that the Na at the surface is either bound as an oxide or hydroxide, or it is incorporated into a thin SiO_2 layer formed by the residual oxygen during annealing in flowing Ar. A Na concentration of about 0.1 at.%, however, is left in the epitaxially regrown region. This concentration clearly exceeds the equilibrium solid solubility of Na in Si, namely 2.4×10^{-3} at.% at 840 K

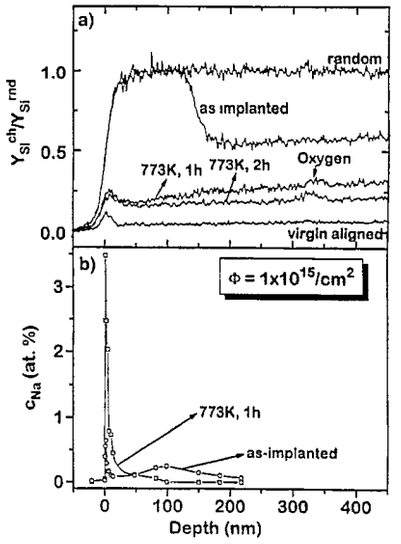

Fig. 4 (a) RBS-C spectra, normalized to the "random" yield, measured with the Si samples implanted with 50 keV Na^+ ions to a fluence of 1×10^{15} cm^{-2} and annealed at 773 K for different annealing times. The given depth scale refers to α-particles scattered at Si atoms. (b) Concentration distributions of Na implanted into Si(100) to fluences of 1×10^{15} cm^{-2} at 50 keV energy and after 1 annealing at 773 K.

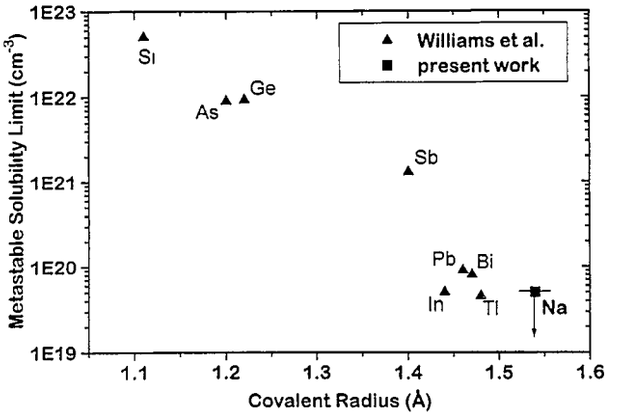

Fig 5 Metastable solubility limit during SPEG of Si at 773 K as a function of the covalent atomic radius of different implanted impurity atoms

[19,20]. However, it fits well into the relationship found by Williams and Short [11] between the metastable solubility limit during recrystallization and the covalent radius of the implanted species, as is shown in Fig. 5. We therefore conclude that the remaining Na atoms are substitutionally incorporated into the epitaxial layer.

Since after 1 h annealing complete epitaxial regrowth was observed, the corresponding regrowth rate of this sample must have been higher than 2.3 nm min^{-1}. This is more than twice the intrinsic regrowth rate of 1 nm min^{-1} at 773 K in self-ion irradiated Si(100) (e.g. in the absence of impurity atoms) [33]. As was also found for other ion species [8–10] implantation of small concentrations of some 0.1 at.% Na obviously enhances the epitaxial regrowth of the Si matrix significantly.

3.2.2. *Intermediate-fluence implantation*

RBS-C spectra of Si samples implanted with 50 keV Na$^+$ at a fluence of 1×10^{16} cm^{-2} and after different heat treatments are displayed in Figs. 6(a) and 7. Fig. 6(b) shows the resulting Na concentration profiles obtained via RNRA. Fig. 6(a) refers to samples annealed for 0.5 and 4 h at 773 K, while Fig. 7 refers to samples annealed for 0.5 h at 753 K and 853 K, respectively. The results are rather similar. The 0.5 h annealings at 753 K and 773 K shift the a/c interface from about 170 nm to about 100 nm, but leave the backscattering yield of this 100 nm thick front layer at the random level. Further annealing at 773 K or 0.5 h annealing at a higher temperature of 853 K do not change the position of the SPEG front but reduce the backscattering yield from the remaining top layer by some 10%. This indicates that the expitaxial regrowth has stopped at about 100 nm depth (i.e. in a region of initially high Na concentration) in favor of the formation of a polycrystalline top layer, which realigns and becomes textured during further annealing.

This interpretation is strongly corroborated by the results of transmission electron microscopy (TEM) performed on a cross-section [34] of the sample annealed for 4 h at 773 K. In Fig. 8(a) a typical TEM image is shown, while in

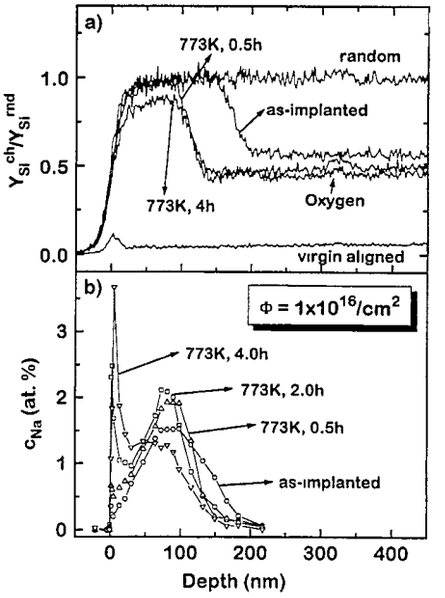

Fig 6 (a) RBS-C spectra, normalized to the "random" yield, measured with the Si samples implanted with 50 keV Na$^+$ ions to a fluence of 1×10^{16} cm^{-2} and annealed at 773 K for different annealing times. The given depth scale refers to α-particles scattered at Si atoms (b) Concentration distributions of Na implanted into c-Si to fluences of 1×10^{16} cm^{-2} at 50 keV energy and after annealings at 773 K for different annealing times

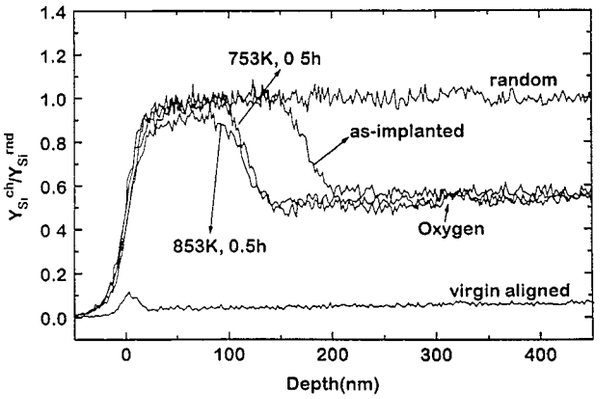

Fig. 7. RBS-C spectra, normalized to the "random" yield, measured with the Si samples implanted with 50 keV Na$^+$ ions to a fluence of 1×10^{16} cm^{-2} and annealed at various temperatures for 0.5 h. The given depth scale refers to α-particles scattered at Si atoms.

Fig. 8(b) the diffraction patterns taken in the regions marked by A and B in Fig. 8(a) are displayed. The depth of the initially induced a/c interface is still indicated by the remaining end-of-range defects [35] and also the epitaxially regrown zone becomes clearly visible. The location of the interfaces and the extension of the sublayers are in good agreement with our RBS-C results. The top-layer has become polycrystalline, as can be nicely seen in the diffraction pattern A, which exhibits a series of spots corresponding to different crystallographic orientations. At higher resolution, as is shown in Fig. 9, fringes become visible in the polycrystalline layer, which indicate that the grains are roughly aligned with

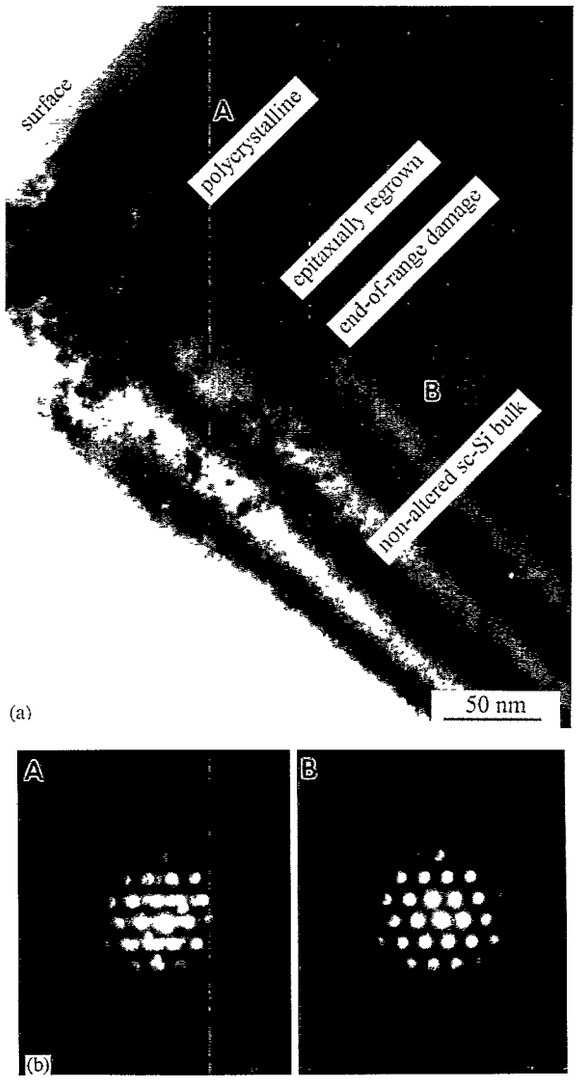

Fig. 8. (a) Bright-field TEM image of a cross-section through the sample implanted with 1×10^{16} Na^+ cm^{-2} and annealed at 773 K for 4 h. (b) Focused diffraction pattern taken in the regions indicated by A and B in (a)

the crystallographic orientation of the bulk, giving rise to the observed small channeling effect.

The evolution of the Na concentration profile during the 773 K annealing cycle is shown in Fig. 6(b), which illustrates the two steps of the Na migration. The as-implanted profile is broadly distributed having its center at 94 nm, a width of 115 nm (FWHM) and a peak concentration of 1.6 at.%, and compares fairly well with the prediction of TRIM95 ($R=99$ nm, $\Delta R=94$ nm). Annealing for 0.5 h at 773 K moves the deeper tail of the implantation profile towards smaller depths, leading to a narrower distribution (peak at 78 nm, width 85 nm, and peak height of 2.0 at.%). In addition, a surface peak starts to develop. Again we note that a small amount of oxygen can be detected in the RBS-C spectra, indicating oxide formation at the surface. After 2 h annealing, the distribution has shifted and narrowed further, while the Na content near

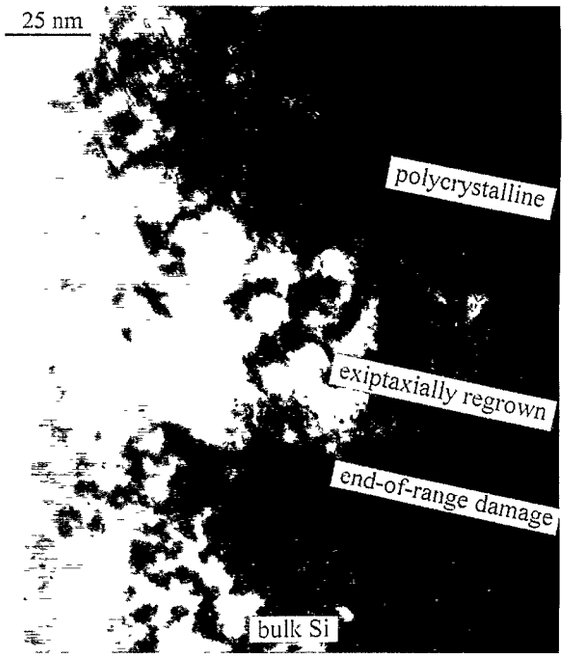

Fig. 9. High-resolution image of the cross-section already shown in Fig. 8(a). Note the fringes in the polycrystalline layer.

the surface has still been increased. Finally, after 4 h of heat treatment at 773 K, a broad Na profile remains with still more Na located near the surface. Note that the Na peak concentration as well as the Na level in the 25–100 nm top layer region (which was found to be polycrystalline) by far exceeds the equilibrium solubility as well as the metastable solubility limit. We therefore conclude that during the first annealing step epitaxial regrowth occurs with an incorporation of about 0.1 at.% Na into the recrystallized material. When the recrystallization proceeds, an increasing Na concentration is accumulated at the a/c interface, because, on the one hand, the a/c front moves towards the maximum of the implantation profile and, on the other hand, the Na in excess of the metastable solubility limit is driven into the amorphous layer. This might lead to the formation of Na precipitates, which strongly retard the epitaxial regrowth such that it can no longer compete with the polycrystallization of the remaining material. During further annealing, the Na precipitates then seem to dissolve by grain boundary diffusion through the polycrystalline layer. At the same time realignment of the polycrystalline layer with respect to the orientation of the bulk occurs, indicated by the small channeling effect described above.

3.2.3. *High-fluence implantation*

We finally discuss the results obtained after implanting 1×10^{17} Na^+ ions cm^{-2} into Si(100) and heating this sample for 1 and 2 h in an argon atmosphere. The RBS-C spectra of this series are shown in Fig. 10(a), while the Na profiles are displayed in Fig. 10(b). As already mentioned above, the peak at the back-edge of the RBS-C spectrum of the as-

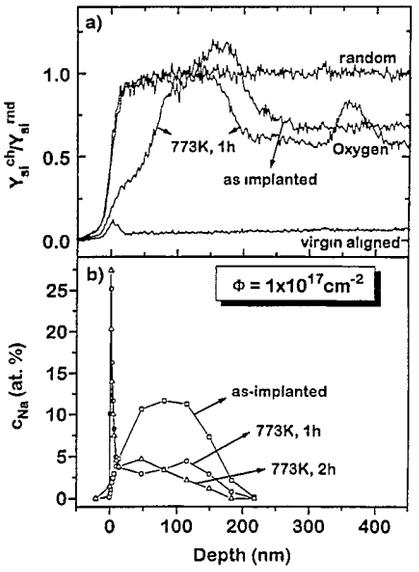

Fig. 10. (a) RBS-C spectra, normalized to the "random" yield, measured with the Si samples after implantation with 50 keV Na^+ ions to a fluence of 1×10^{17} cm^{-2} and annealed at 773 K for 1 h. The given depth scale refers to α-particles scattered at Si atoms. (b) Concentration distributions of Na implanted into c-Si to fluences of 1×10^{17} cm^{-2} at 50 keV energy and after annealings at 773 K for different annealing times.

implanted sample is due to backscattering at the implanted Na atoms, and the shift of the back-edge after 773 K annealing (1 h) is merely because more than 60% of the initially Gaussian-like distributed Na atoms have disappeared. Thus almost no epitaxial regrowth can be detected. Instead, a nearly 50 nm thick SiO_2 layer has formed on top the sample after annealing in the Ar atmosphere. Obviously, the very large amount of Na accumulated at the surface during annealing is not only oxidized itself but also induces an instability of the Si surface against oxidation. In contrast to the samples implanted with lower fluences, no shift occurs of the Na profile towards smaller depths, most probably because of the lack of expitaxial regrowth.

3.3. Sodium release

As was already mentioned above and is illustrated in Fig. 1 for the 60 keV and the 200 keV Na implantation the thermally induced release of Na from the implantation site in Si starts above 773 K. In contrast to the samples annealed in Ar, no surface peak was observed in the Na profiles of these vacuum annealed samples. Obviously, because of the absence of oxygen neither Na nor Si oxide can form and the sodium evaporates into the vacuum. (Note that the melting point of Na, $T_m=371$ K, is far below the processing temperature.) As discussed in Section 3.2, a two-step release process must be considered:

Step 1: segregation. During epitaxial recrystallization of Si, which starts at about 773 K, the Na content in excess of the metastable solubility limit is driven out of the regrowth zone into the remaining amorphous material near the a/c interface.

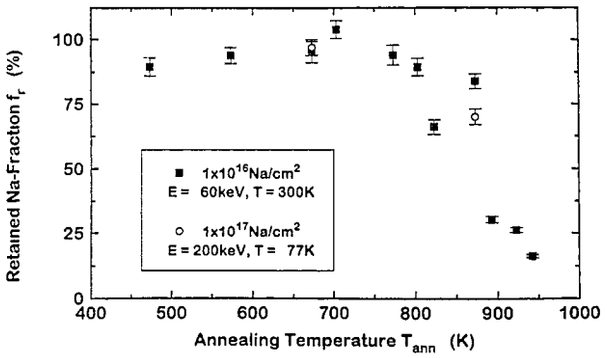

Fig 11. Fraction f_r of the initially implanted Na atoms, which remains in the implanted zone after thermal treatment, as function on the annealing temperature after 60 keV (RT) and the 200 keV (LNT) implantation (annealing time 1 h).

This accumulation of Na atoms probably results in the formation of precipitates, which strongly retard and finally stop the epitaxial recrystallization in favor of polycrystalline regrowth of the remaining top layer.

Step 2: grain boundary diffusion. During further annealing, these precipitates dissolve via grain boundary diffusion of Na through the polycrystalline layer. Arriving at the surface, Na is either oxidized or evaporated into the vacuum.

In Fig. 11 the retained Na fraction f_r (i.e. that fraction of the initially implanted Na atoms which remains in the implantation zone after heat treatment (20–200 nm for 60 keV, 20–600 nm for 200 keV)) is plotted as a function of the annealing temperature for 1 h vacuum annealing of the 60 and 200 keV Na implanted samples. For both implantation energies f_r stays essentially constant up to 800 K, namely $f_r=1.0$, and drops rapidly to $f_r=0.18$ at 943 K. At the critical temperature $T_c=885(30)$ K, which is 47(2)% of the melting point of Si, half of the Na content has diffused out of the sample and being evaporated into the vacuum. Again it becomes clear that outdiffusion of Na from Si does not occur in the amorphous phase, but either by a pushing out mechanism at the expitaxial recrystallization front [3,11] (for low Na contents) or by grain boundary diffusion if a polycrystalline top layer has formed (at high implantation fluences).

The observed two-step Na release in Si is very similar with what was observed in Na-implanted polycrystalline bcc and fcc metals [21,36]. In these cases outdiffusion of Na also occurs in two stages. First, the Na distribution shifts towards the depth of maximum damage and obviously segregates into the open volume created by vacancy type defects. Further annealing at increasing time or temperature then results in Na migration towards the surface and evaporation into the vacuum. Uhrmacher and Lieb [36] have reported an empirical relationship between the critical temperature T_c, where half of the implanted Na has left the sample and the melting point T_m of the metal. They found the ratio $T_c/T_m=0.70(2)$ for fcc metals and $T_c/T_m=0.53(2)$ for bcc metals. The latter value is very similar to that observed in the present work, although the processes must differ a little, since the metals,

of course, were not amorphized by ion bombardment. However, in both cases the excessive insoluble Na is segregating into the more open structure of the sample (defects in metals, amorphous phase in Si) and afterwards released to the vacuum by grain boundary diffusion.

3.4. Trapping and release of hydrogen

In addition to the release of the implanted Na we have investigated the trapping and release of hydrogen at the ion beam modified zone of our samples. Fig. 12 shows the hydrogen profiles measured in 60 keV Na-implanted Si(100) after annealing at various temperatures. It can be seen that, besides the always present surface peak, hydrogen is almost homogeneously incorporated into the amorphous layer during annealing at 703 K. The concentration of about 0.04 at.% is at least four times larger than the background level observed in the non-modified depths and after 573 K annealing. The H-profile nicely resembles the shape of the as-implanted amorphous layer in Fig. 7, when extrapolated to 60 keV ion energy. Subsequent annealing at 773 K then results in the release of the previously trapped hydrogen atoms. In Fig. 13 the H-content in the modified and the non-modified region of two 60 keV Na implanted samples is shown as a function of the annealing temperature for subsequent 1 h annealings. While no changes can be detected in the non-modified part of the sample, the H content starts to strongly increase in the amorphized zone above about 573 K and reaches a maximum at 703 K. Annealing at higher temperatures results in a release of hydrogen and at 773 K the H concentration has almost reached the background level. Note that the recrystallization of Si already occurs at 753 K (compare Fig. 7).

Obviously, under the given conditions, amorphous Si exhibits a much higher H solubility (≥ 0.04 at.% at 703 K based on our data) as compared to its crystalline counterpart (≤ 0.007 at.% based on our data), and will thus be "decorated" by hydrogen as soon as it becomes available.

In the present case, it is not clear whether the H atoms come from the Si bulk or from water and hydrocarbide contaminations at the surface. The latter source, however, seems

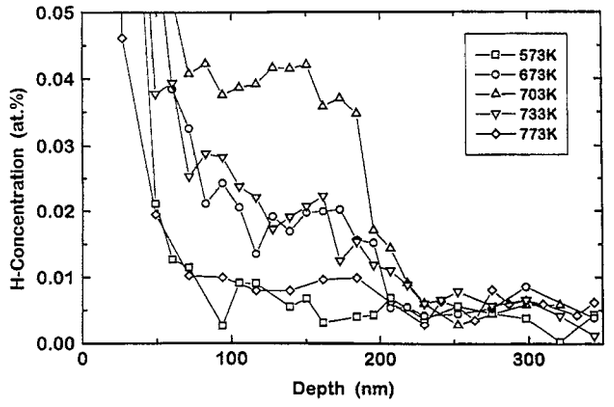

Fig. 12. Hydrogen profiles of a 60 keV Na implanted sample taken after subsequent 1 h annealing at 573 K, 703 K and 773 K.

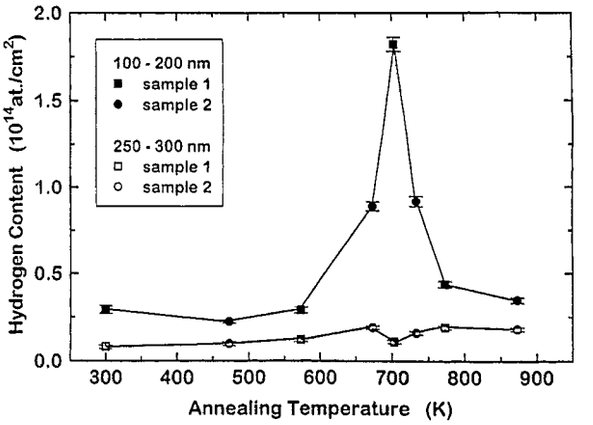

Fig 13 Integrated H content in part of the modified (100–200 nm) and part of the non-modified depth (250–300 nm) of 60 keV Na implanted and subsequently annealed samples as function of the annealing temperature (annealing time 1 h)

to be the most probable in the view of the strong surface peak observed in the H profiles. During recrystallization the H solubility is strongly reduced and, like for the insoluble Na, the hydrogen is pushed out of the sample. Careful inspection of the profiles shown in Fig. 12, however, shows that there is still some hydrogen in excess after 773 K annealing, which might have been trapped by the residual, dislocation type defects in the epitaxially regrown layer or at the grain boundaries of the polycrystalline top layer.

4. Summary and conclusions

The implantation and thermal annealing of essentially insoluble Na in Si(100) and depth profiling of the Na and H concentration distributions via RNRA and of the damaged lattice structure via RBS-C allowed us to study the competition of epitaxial (SPEG) and polycrystalline regrowth of Si and its relationships with the diffusion of the implanted Na atoms as a function of the implanted Na fluence. Furthermore trapping of hydrogen in the amorphized region and its release at the onset of recrystallization was observed. Fluences of 10^{15} Na cm^{-2}, leading to maximum Na concentrations of about 0.2 at.% result in an enhanced regrowth rate as compared to the intrinsic value, and complete epitaxial regrowth occurs. The substitutionally incorporated Na concentration was estimated as 0.1 at.%, which agrees well with the relationship found between the metastable solubility limit of implanted impurities and their covalent atomic radius. At higher Na concentrations, SPEG is strongly retarded in favor of polycrystalline regrowth. In these cases only partial epitaxial recrystallization occurs and a polycrystalline layer forms on top of the sample. The Na atoms in excess of the metastable solubility limit are assumed to form small segregates which finally dissolve by grain boundary diffusion through the polycrystalline layer. This two-step Na release is similar to that found in Na-implanted metals and so is the ratio 0.47(2) between the temperature $T_c = 885(30)$ K,

where half of the implanted Na atoms have left the sample, and the melting point of Si.

It will be interesting to check whether the effect of H-trapping and release during amorphization and recrystallization of Si might be used to monitor the irradiation induced amorphization of polycrystalline samples, which by no means would be possible with RBS-C.

Acknowledgements

This work has been supported by the Deutsche Forschungsgemeinschaft (DFG), Deutscher Akademischer Austauschdienst (DAAD), and Academy of Finland. We are most grateful to R. Ingren, H. Sepponen and D. Purschke for help and perfectly operating the accelerators.

References

[1] J.W Mayer, L. Eriksson and J.A. Davies, *Ion Implantation in Semiconductors,* Academic Press, New York, 1970.
[2] L. Csepregi, J W. Mayer and T.W. Sigmon, *Phys. Lett., 54A* (1975) 157.
[3] J.S. Williams, *Nucl. Instrum. Methods, 209/210* (1982) 219.
[4] L Csepregi, E.F. Kennedy, J.W. Mayer and T.W. Sigmon, *J. Appl. Phys , 49* (1978) 3906.
[5] L Csepregi, E.F. Kennedy, J W Mayer and T.W. Sigmon, *J. Appl. Phys , 48* (1977) 4243.
[6] S.U Campasino and A.E. Barbarino, *Appl. Phys., 25* (1981) 153.
[7] E F Kennedy, L Csepregi, J W Mayer and T.W. Sigmon, *J. Appl. Phys., 48* (1977) 4241.
[8] J S Williams and R.G. Elliman, *Appl Phys. Lett., 37* (1980) 829.
[9] J S. Williams and R.G. Elliman, *Appl. Phys. Lett., 40* (1982) 266.
[10] J S. Williams and R.G. Elliman, *Nucl. Instrum. Meth., 183* (1981) 758
[11] J S. Williams and K.T. Short, in Choyke and Picraux (eds.), *Metastable Materials Production by Ion Implantation,* North-Holland, Amsterdam, 1982.
[12] G.L. Olson and J.A. Roth, *Mater. Sci. Rep., 3* (1988) 1.
[13] F. Spaepen and D. Turnbull, *AIP Conf. Ser., 50* (1979) 73.
[14] F. Spaepen and D Turnbull, in Poate and Mayer (eds), *Laser Processing of Semiconductor Structures,* Academic Press, New York, 1982.
[15] K Sheshan and E.P. EerNisse, *Appl. Phys. Lett , 33* (1978) 21.
[16] J R. Patel, L Testardi and P E. Freeland, *Phys Rev., B15* (1977) 4121.
[17] P.B. Hirsch, in J. Narayan and T Y Tan (eds), *Defects in Semiconductors,* North Holland, Amsterdam, 1981.
[18] M. Uhrmacher, K Pampus, F.J. Bergmeister, D. Purschke and K P Lieb, *Nucl Instrum Meth., B9* (1985) 234
[19] J O McCaldin, M.J. Little and A E Widmer, *J. Phys Chem Solid, 26* (1965) 1199.
[20] L. Svob, *Phys. Status Solidi, I* (1) (1964) K1–K3.
[21] N Scapellato, M. Uhrmacher and K.P. Lieb, *J. Phys F, Metal. Phys., 18* (1988) 677.
[22] P Haussalo, K P. Lieb, W. Bolse, C. Illgner and J. Keinonen, *Proc. of E-MRS* (1996) in press K.P. Lieb, P. haussalo, W Bolse, C. Illgner, J. Keinonen and M. Niederdrenk, *Thin Solid Films* (1997) in press
[23] F. Harbsmeier, *Diploma Thesis*, Göttingen 1996, unpublished.
[24] W.K Chu, J.W. Mayer and M -A Nicolet, *Rutherford Backscattering Spectrometry,* Academic Press, New York, 1978
[25] K P Lieb, W. Bolse, T Corts, T. Kacsich, A Kehrel and M. Uhrmacher, in W R Hoff (ed), *Capture Gamma Ray Spectroscopy,* Am. Inst Physics, New York, 1991, p 983
[26] W. Bolse, *Mater. Sci. Eng., R12* (1994) 53.
[27] P. Torri, J. Keinonen and K Nordlund, *Nucl. Instrum Meth , B84* (1994) 105.
[28] J.F. Ziegler, Hydrogen-stopping powers in all elements, *The Stopping and Ranges of Ions in Matter*, Vol. 3, Pergamon Press, New York, 1977
[29] J F. Ziegler, J.P. Biersack and U. Littmark, *The Stopping and Range of Ions in Solids,* Vol 1, Pergamon Press, New York, 1985.
[30] W Bolse, J Conrad, F Harbsmeier, M. Borowski and T. Rödle, *Mat. Sci. Forum* (1997) in press.
[31] W Wesch, E Wendler, J. Kaczanowski and A Turos, *Nucl. Instrum. Meth., B85* (1994) 533.
[32] C.E. Mortimer, *Chemistry*, Wadsworth Publishing, Belmont CA, 1986.
[33] S.S. Lau, *J. Vac. Sci. Technol., 15* (1978) 1656.
[34] J.C Bravman and R. Sinclair, *J. Electr. Microsc. Tech , 1* (1984) 53.
[35] K.S. Jones, S. Prussin and E.R. Weber, *Appl. Phys., A45* (1988) 1.
[36] A. Kehrel, K P. Lieb and M Uhrmacher, Mat. Sci Eng. A 115 (1989) 43; M. Uhrmacher and K.P. Lieb, *Nucl Instrum. Meth., B68* (1992) 175